Article

Determination of Material Parameters of PDMS Material Models by MATLAB

Jate Phothiphatcha[a] and Tumrong Puttapitukporn[b,*]

Department of Mechanical Engineering, Faculty of Engineering, Kasetsart University, Bangkok 10900, Thailand
E-mail: [a]jphothiphatcha@gmail.com, [b,*]fengtop@ku.ac.th (Corresponding author)

Abstract. Generally, material constants and their corresponding stability regions of hyperelastic constitutive models can be obtained by well-known commercial software. Nonetheless, reproduction of engineering stress-strain curves from these software do not accurately represent of the uniaxial testing data of a Polydimethylsiloxane material (PDMS). This research aimed to develop *PP* algorithm, which are MATLAB codes, used to determinate hyperelastic material constants and their stability regions from uniaxial testing data of PDMS material. Hyperelastic constitutive models composed of Neo-Hookean; 3, 5, and 9 parameters Mooney-Rivlin; 2nd and 3rd order Yeoh; and 1st, 2nd and 3rd order Ogden. Moreover, the accuracies of our results were evaluated by the residual sum of squares (RSS) between testing data and hyperelastic models and compared with ones of ANSYS. In Neo-Hookean and Ogden models, the *PP* algorithm effectively determined material constants from the uniaxial testing data in which their RSS were lower than ones from ANSYS while the strain limit ranges were comparable. However, in Mooney-Rivlin and Yeoh models, the *PP* algorithm obtained lower RSS but had narrower strain limit ranges than ones from ANSYS. Finally, the Ogden 3rd order model is the accurate constitutive model for PDMS since it obtained not only low RSS but also no strain range limit.

Keywords: Hyperelastic material models, finite element analysis, MATLAB, PDMS, ANSYS.

1. Introduction

Hyperelastic constitutive models are mathematical models that design to simulate behaviors of rubber-like materials, such as silicone, soft tissue, skin, polymer, leather etc. Many researchers have focused on determination of hyperelastic materials parameters from laboratory testing data. Ali et al. [1] reviewed constitutive models for rubber-like materials. López-Campos et al. [2] applied genetic algorithm in MATLAB to determine material constants in hyperelastic constitutive models and compared accuracies of these results with ANSYS and ABAQUS program. Kindo et al. [3] studied on selection and validation of hyperelastic finite element model for analysis of silicone rubber. They found that the most accurate hyperelastic material model was Yeoh and Mooney-Rivlin models. Tobajas et al. [4] focused on comparative study of hyperelastic constitutive models for an automotive shaft seal material made of Santoprene 101-73. The authors used of R-Squares (correlation coefficient) to determine quality of each hyperelastic constitutive model. They found that Mooney-Rivlin model had the highest R-squared. Mansouri and Darijani [5] developed the constitutive model of isotropic hyperelastic materials in an exponential framework using a self-contained approach and used residual sum of squares (RSS) for comparison the accurate each model. Gorash, Comlekci, and Hamilton [6] developed a CAE-based application with a convenient GUI for identification and verification of material parameters for hyperelastic models available in the current release of the FE-code ANSYS Mechanical APDL. Kumar, and Rao [7] studied determination and physical interpretation of material constants in Mooney-Rivlin model. Marckmann, and Verron [8] evaluated materialparameters and the stretch range of hyperelastic models for rubber-like materials. Elgström [9] studied practical implementation of hyperelastic material methods in FEA models using MATLAB program. Iniguez-Macedo et al. [10] developed finite element model updating by combining multi-responses of force-displacement curves from tensile, plane stress, compression, volumetric compression and shear tests to optimize hyper-elastic materials characterization. Kim et al. [11] comparative study of several material models for prediction of hyperelastic properties of silicone-rubber and soft tissues in ABAQUS. Ruggiero et al [12] used inverse method to determine material properties of soft tissues using Mooney-Rivlin model in ABAQUS.

Finite element analyses of structures made of hyperelastic materials under loading are also interesting designing issues. Mansouri, Darijani, and Baghani [13] studied simulation deflected shapes of the inflation experiment of silicone rubber with various constitutive model in ABAQUS and measures accuracies of each constitutive models by RSS. Liu et al. [14] studied uniaxial tension of thin rubber liner sheets and hyperelastic model investigation. They found that the Mooney–Rivlin model up to the second order and the Ogden model capture the constitutive behaviour of both the silica-filled and the Kevlar-filled rubber sheets quite accurate. Pawlikowski [15] studied non-linear approach in visco-hyperelastic constitutive modelling of polyurethane nanocomposite. They found that the mean relative error of the Ogden model and the Mooney-Rivlin model was less than 10 %. Zhong, and Peters [16] studied hyperelastic tissue model under compressive loading in ABAQUS.

Wang, Ma, and Wang [17] developed the finite element stratification method for a polyurethane jounce bumper, which was divided into three regions (the 'skin layer', the 'transition layer', and the 'core area'), having different material properties in ABAQUS. The coefficients of the Ogden model obtained by nonlinear least-squares fitting by Levenberg-Marquard algorithm was applied to fit in ABAQUS.

Drucker stability condition requires energy functions obeying to ensure stable material responses for all strain rates which can be derived from the tangential material stiffness matrix (D). Thus, material models will be stable if D is positive definite matrix. Oden, and Fung [18] summarized the suitable range of strain in hyperelastic constitutive models. The Neo-Hookean model gives a good correlation with the experimental data up to 40% strain in uniaxial tension. The Mooney-Rivlin model shows a good agreement with tensile test data up to 100% strains. The Yeoh model was suitable for wider range of strains and useful in capturing different modes of deformation. Finally, the Ogden model gives a good correlation with test data in simple tension up to 700%. Upadhyay, Subhash, and Spearot [19] developed thermodynamics-based stability criteria for constitutive equations of isotropic hyperelastic solids. They found that stability of the Neo-Hookean model requied $C_{10} > 0$ for all deformation mode while the stability of Mooney-Rivlin 2 parameter model, required $C_{10} + C_{01} > 0$ and $C_{01} > 0$ for uniaxial compression and $C_{10} + C_{01} > 0$ and $C_{10} > 0$ for uniaxial tension. Liu [20] formulated thermodynamic stability criterion for an isothermal uniaxial test and determined limiting tensile and compressive tests strain for the Mooney-Rivlin model. They found that the uniaxial stress-strain curve become unstable if the curve was concave-downward.

Hydrophobic surfaces have the ability of water repellent which can be coated on medical devices and marine structures. These surfaces are generally fabricated from the soft lithography technique which creates micropillars on a substrate made of Polydimethylsiloxane (PDMS). Since PDMS has low surface energy, non-toxic, non-flammable and good biocompatibility. Thanakhun and Puttapitukporn [21] studied the structural behaviour of micropillars fabricated from a core made of PUA material coated with a PDMS material and compared their lateral strength under shear loadings in ANSYS Mechanical APDL program. The authors found that the PUA core coated with 100 nm-thick PDMS micropillar illustrated better lateral strength than pure PDMS micropillar. Pakawan et al. [22] studied effects of decreasing the substrate thicknesses on the mechanical

behaviour of PDMS micropillar sheets under compressive loading in ANSYS Mechanical APDL program.

This research aimed to propose the *PP* algorithm which is the effective MATLAB algorithm used to determinate material constants and strain limit ranges in hyperelastic constitutive models of PDMS materials. These constitutive models compose of Neo-Hookean, Yeoh, Mooney-Rivlin, and Ogden. Finally, accuracies of engineering stress-strain curves reproduction were evaluated by RSS between testing data and hyperelastic models and were compared with ones of the commercial finite element program, ANSYS.

2. Theory

2.1. Hyperelastic Material Models

Hyperelastic material models are used to formulate the nonlinear large deformation behaviour of elastomer materials which are implemented in the most finite element software. Here, the stress-strain relation is derived from the strain energy density function (W), unlike linear elastic materials in which the stress-strain relationship is given by Young's modulus and Poisson ratio. Figure 1 shows the difference of the stress-strain relation of elastic and hyperelastic materials. Moreover, the hyperelastic materials can be used to derive nonlinear constitutive models in terms of 1st, 2nd and 3rd invariants (I_1, I_2, and I_3), such as Neo-Hookean, Mooney-Rivlin, and Yeoh models. However, some constitutive models are not written in term of these invariants. For example, the Ogden model expresses its constitutive model in term of a stretch ratio.

2.1.1. Invariants

The invariants of the green deformation tensor consist of the invariants of I_1, I_2, and I_3. These invariants can be written in term of the principal stretch ratios of $\lambda_1, \lambda_2,$ and λ_3 as shown in Eqs. (1)-(4).
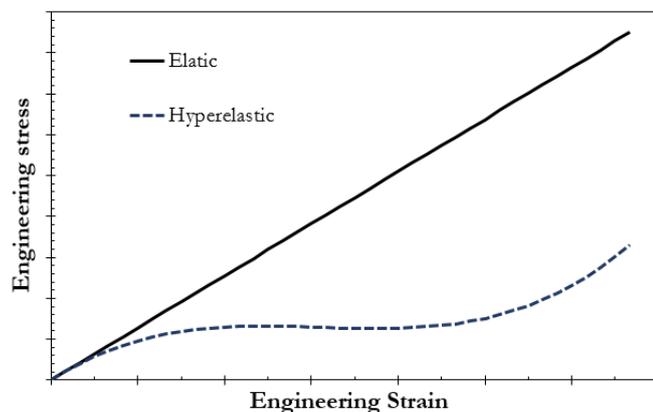
Fig. 1. Engineering stress-strain curves of elastic and hyperelastic materials.

$$I_1 = \lambda_1^2 + \lambda_2^2 + \lambda_3^2 \qquad (1)$$

$$I_2 = \lambda_1^2 \lambda_2^2 + \lambda_1^2 \lambda_3^2 + \lambda_2^2 \lambda_3^2 \qquad (2)$$

$$I_3 = \lambda_1^2 \lambda_2^2 \lambda_3^2 \qquad (3)$$

The stretch ratio in the i-direction can be written in term of the engineering strain as

$$\lambda_i = 1 + \varepsilon_i \qquad (4)$$

For incompressible materials, the third invariant I_3 equals 1. The stretch ratios of λ_1, λ_2, and λ_3 obtain from elastomer material testing which composes of the uniaxial test, equibiaxial test, and planar test as shown in Fig. 2. The constitutive models of these testing results are influenced by both I_1 and I_2. In this research, we focused our study on determination of material parameters of incompressible materials from the uniaxial testing. Therefore, the three principal stretch ratios are given as $\lambda_1 = \lambda$, $\lambda_2 = \lambda_3 = \lambda^{-0.5}$, and $\lambda = 1 + \varepsilon_1$. As result, the three invariants are written in Eqs. (5)-(6).

$$I_1 = \lambda^2 + 2\lambda^{-1} \qquad (5)$$
$$I_2 = 2\lambda + \lambda^{-2} \qquad (6)$$

For equibiaxial test, the three principal stretch ratios are given as $\lambda_1 = \lambda_2 = \lambda$, $\lambda_3 = \lambda^{-2}$, and $\lambda = 1 + \varepsilon_1$ (since $\varepsilon_1 = \varepsilon_2$). Invariants are shown in Eqs. (7)-(8).

$$I_1 = 2\lambda^2 + \lambda^{-4} \qquad (7)$$
$$I_2 = 2\lambda^{-2} + \lambda^4 \qquad (8)$$

For planar test, the three principal stretch ratios are given as $\lambda_1 = \lambda$, $\lambda_2 = 1$, $\lambda_3 = \lambda^{-1}$, and $\lambda = 1 + \varepsilon_1$. Invariants are shown in Eq. (9).

$$I_1 = I_2 = \lambda^2 + \lambda^{-2} + 1 \qquad (9)$$

2.2. Strain Energy Density Function (W)

2.2.1. Neo-Hookean model

The Neo-Hookean model is used for predicting the nonlinear stress-strain behaviour of rubber-like materials under large deformation, in contrast with the linear elastic behaviour defined by Hooke's law. It can be written as in Eq. (10).

$$W = C_{10}(I_1 - 3) \qquad (10)$$

where C_{10} is a material constant.

2.2.2. Mooney-Rivlin model

The Mooney-Rivlin model is developed from the Neo-Hookean model. The model is popular for modelling the large strain nonlinear behaviour of incompressible materials. It can be expressed in terms of the first and second invariants as Eq. (11).

$$W = \sum_{i+j=1}^{n} C_{ij} \left(I_1 - 3\right)^i \left(I_2 - 3\right)^j \qquad (11)$$

where n is the number of material constants and C_{ij} is the material constant.
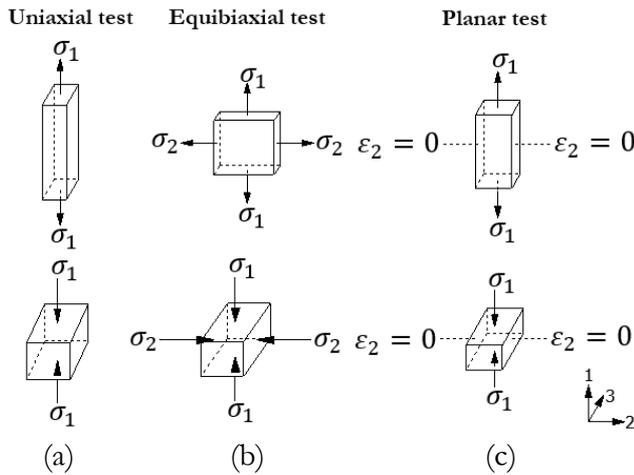
Fig. 2. Hyperelastic material testing: (a) uniaxial test, (b) equibiaxial test, and (c) planar test.

2.2.3. Yeoh model

The Yeoh model is a phenomenological model for the deformation of nearly incompressible and nonlinear elastic materials, such as rubbers. It is also called the reduced polynomial model. The strain energy density function depends only on the first strain invariant, I_1. It can be written in Eq. (12).

$$W = \sum_{i=1}^{n} C_{ij} \left(I_1 - 3\right)^i \qquad (12)$$

where n is the number of material constants and C_{ij} is the material constant.

2.2.4. Ogden model

The Ogden model is a general hyperelastic model in which its strain energy density is expressed in terms of the principal stretches. The strain energy density can be written in Eq. (13).

$$W = \sum_{i=1}^{n} \frac{\mu_i}{\alpha_i} \left(\lambda_1^{\alpha_i} + \lambda_2^{\alpha_i} + \lambda_3^{\alpha_i} - 3\right) \qquad (13)$$

where n is the number of material constants, μ_i and α_i are material constants.

2.3. Determination of Stresses

The engineering stress can be derived from a derivative of the strain energy density function by the stretch ratio as written in Eq. (14).

$$\sigma_i = \frac{\partial W}{\partial \lambda_i} \qquad (14)$$

where σ_i and λ_i are an engineering stress and a stretch ratio in the i-direction respectively. In addition, many constitutive models are written in term of the invariants. Therefore, if W is a function of I_1 and I_2, the engineering stress in the i-direction can be rewritten as in Eq. (15).

$$\sigma_i = \frac{\partial W}{\partial I_1} \frac{\partial I_1}{\partial \lambda_i} + \frac{\partial W}{\partial I_2} \frac{\partial I_2}{\partial \lambda_i} \qquad (15)$$

2.3.1. Neo-Hookean model

For a uniaxial loading in the 1-direction, the engineering stress derived from the Neo-Hookean model depends only on the 1st invariant so that it can be derived from Eq. (15) by neglecting the 2nd invariant term. Therefore, the engineering stress can be written in Eq. (16).

$$\sigma_1 = C_{10} \left(2\lambda - 2\lambda^{-2}\right) \qquad (16)$$

2.3.2. Mooney-Rivlin model

Engineering stresses derived from the Mooney-Rivlin model depends on both the 1st invariant and 2nd invariant. By substituting the strain energy density model in Eq. (15). The engineering stress can be expressed as:

3-parameters

$$\sigma_1 = \begin{cases} 2C_{10}\left(\lambda - \lambda^{-2}\right) + 2C_{01}\left(1 - \lambda^{-3}\right) \\ +6C_{11}\begin{pmatrix} \lambda^2 - \lambda - 1 + \lambda^{-2} \\ \lambda^{-3} - \lambda^{-4} \end{pmatrix} \end{cases} \qquad (17)$$

5-parameters

$$\sigma_1 = \begin{cases} 2C_{10}\left(\lambda - \lambda^{-2}\right) + 2C_{01}\left(1 - \lambda^{-3}\right) \\ +6C_{11}\left(\lambda^2 - \lambda + \lambda^{-2} + \lambda^{-3} - \lambda^{-4} - 1\right) \\ +4C_{20}\left(\lambda^3 - 3\lambda + 3\lambda^{-2} - 2\lambda^{-3} + 1\right) \\ +4C_{02}\left(2\lambda - \lambda^{-2} + 3\lambda^{-3} - \lambda^{-5} - 3\right) \end{cases} \qquad (18)$$

9-parameters

$$\sigma_1 = \left\{ \begin{array}{l} 2C_{10}\left(\lambda - \lambda^{-2}\right) + 2C_{01}\left(1 - \lambda^{-3}\right) \\ +6C_{11}\left(\lambda^2 - \lambda + \lambda^{-2} + \lambda^{-3} - \lambda^{-4} - 1\right) \\ +4C_{20}\left(\lambda^3 - 3\lambda + 3\lambda^{-2} - 2\lambda^{-3} + 1\right) \\ +4C_{02}\left(2\lambda - \lambda^{-2} + 3\lambda^{-3} - \lambda^{-5} - 3\right) \\ +2C_{12}\left(\begin{array}{l} 8\lambda^3 - 18\lambda^2 - 3\lambda - 3\lambda^{-2} - 27\lambda^{-3} \\ +18\lambda^{-4} + 6\lambda^{-5} - 5\lambda^{-6} + 24 \end{array}\right) \\ +2C_{21}\left(\begin{array}{l} 5\lambda^4 - 6\lambda^3 - 18\lambda^2 + 27\lambda \\ -24\lambda^{-2} + 3\lambda^{-3} + 18\lambda^{-4} - 8\lambda^{-5} + 3 \end{array}\right) \\ +2C_{30}\left(\begin{array}{l} 3\lambda^5 - 18\lambda^3 + 9\lambda^2 + 27\lambda - 27\lambda^{-2} \\ +36\lambda^{-3} - 12\lambda^{-4} - 18 \end{array}\right) \\ +2C_{03}\left(\begin{array}{l} 12\lambda^2 - 36\lambda + 18\lambda^{-2} - 27\lambda^{-3} \\ -9\lambda^{-4} + 18\lambda^{-5} - 3\lambda^{-7} + 27 \end{array}\right) \end{array} \right\} \quad (19)$$

2.3.3. Yeoh model

Engineering stress derived from the Yeoh model depends only on the 1st invariant. By substituting the strain energy density model in Eq. (15) and neglecting the 2nd invariant term, the engineering stress can be written in Eq. (20).

$$\sigma_1 = \sum_{i=1}^{n} 2iC_{i0}(\lambda - \lambda^{-2})(\lambda^2 + 2\lambda^{-1} - 3)^{i-1} \quad (20)$$

2.3.4. Ogden model

Engineering stress derived from the Ogden model does not depend on both I_1 and I_2, such that the engineering stress can be determined by substituting the strain energy density function into Eq. (14) as shown in Eq. (21).

$$\sigma_1 = \sum_{i=1}^{n} \mu_i \left(\lambda^{\alpha_i - 1} - \lambda^{-0.5\alpha_i - 1} \right) \quad (21)$$

2.4. Drucker Stability Conditions

The stability region of each constitutive model can be determined from the Drucker stability condition for the first three modes of deformation. The condition requires that the changes of the true stress and true strain are satisfied in the inequality as shown in Eq. (22).

$$d\sigma : d\varepsilon > 0 \quad (22)$$

For isotropic hyperelastic materials, the inequality can be represented in terms of the principal stresses and strains as given in Eq. (23).

$$d\sigma_1 d\varepsilon_1 + d\sigma_2 d\varepsilon_2 + d\sigma_3 d\varepsilon_3 > 0 \quad (23)$$

2.5. Residual Sum of Squares

The residual sum of squares (RSS) measures of errors remaining between the model function and the data set. It is used as an optimality criterion in the parameter selection and the model selection which can be calculated by Eq. (24).

$$RSS = \sum_{i=1}^{N} \left(\sigma_i - \sigma \right)^2 \quad (24)$$

where σ_i is the engineering stress obtained from the experimental data, σ is the engineering stress obtained from hyperelastic constitutive models, and N is the number of a data set.

3. Methodology

The *PP* algorithm, named after two researchers, J. Phothiphatcha and T. Puttapitukporn, which is written in MATLAB program for determining material parameters and their strain limit ranges from uniaxial testing data of hyperelastic materials. The hyperelastic models consist of Neo-Hookean; 3, 5, and 9 parameters Mooney-Rivlin; 2nd and 3rd order Yeoh; and 1st, 2nd, and 3rd order Ogden. The *PP* algorithm uses the polynomial function to create the smooth and continuous function from the uniaxial testing data. Then, the specified pairs of the fitted engineering stress-strain data are selected which are equal to the number of material constants in each hyperelastic model. After that, the system of equations can be formulated for determining the material constants. Finally, the stability region is determined from the Drucker stability criterion.

3.1. Uniaxial Test Data

Experimental data [21, 22] of tensile and compressive tests on testing specimens made of PDMS material having the PDMS monomers to a curing agent ratio of 10:1 are shown in Figs. 3-4. The engineering stress and strain curves reproduced from various constitutive models by the ANSYS program are shown in Figs. 3-4.
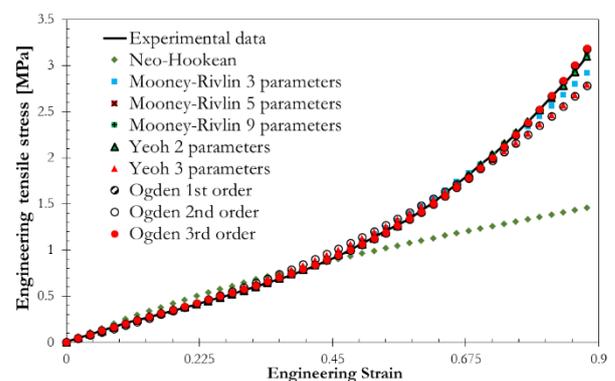
Fig. 3. Comparison of engineering tensile stress and strain

curves obtained from the experimental data and various constitutive models by the ANSYS program.
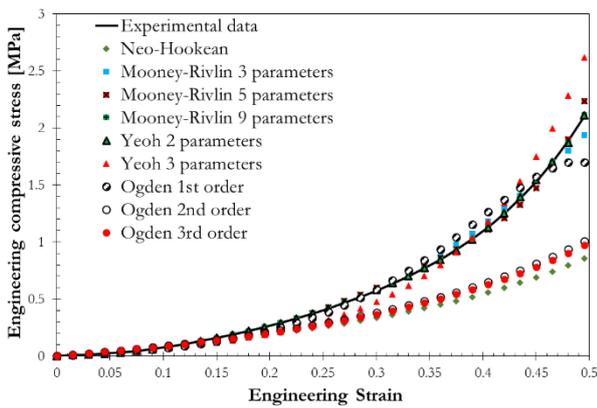
Fig. 4. Comparison of engineering compressive stress and strain curve obtained from the experimental data and various constitutive models by the ANSYS program.

3.2. Determination of Material Constants

3.2.1. Curve fitting

Uniaxial experimental data are often unsmooth curve which necessary to fit curve by using Polynomial function. This equation is shown in Eq. (25) and the coefficients can be determine in Eq. (26), by define as

$$\sigma_{Fit} = a_0 + a_1\varepsilon + a_2\varepsilon^2 + \ldots + a_n\varepsilon^n \qquad (25)$$

$$\begin{bmatrix} n & \sum\varepsilon & \cdots & \sum\varepsilon^n \\ \sum\varepsilon & \sum\varepsilon^2 & \cdots & \sum\varepsilon^{n+1} \\ \vdots & \vdots & \vdots & \vdots \\ \sum\varepsilon^n & \sum\varepsilon^{n+1} & \cdots & \sum\varepsilon^{2n} \end{bmatrix} \begin{bmatrix} a_0 \\ a_1 \\ \vdots \\ a_n \end{bmatrix} = \begin{bmatrix} \sum\sigma_i \\ \sum\varepsilon\sigma_i \\ \vdots \\ \sum\varepsilon^n\sigma_i \end{bmatrix} \qquad (26)$$

where σ_{Fit} is the fitted engineering stress, σ_i is the engineering stress obtained from experimental data, and ε is the engineering strain.

3.2.2. Data selection

After the uniaxial experimental data are fitted by the polynomial function, the strain range T is equally divided by the number of strain intervals which gives an interval length of L as shown in Eq. (27).

$$L = \frac{T}{n} \qquad (27)$$

where n is number of material constants in constitutive models. However, this proposed procedure is suitable for Mooney-Rivlin, Yeoh and Ogden models. The Neo-Hookean model has only one material constant C_{10}; therefore, it must be used different procedure to determine its material constant.

The uniaxial testing data will be accurately matched to the fitted data as shown in Fig. 5. $\sigma_{Fit}^{\{i\}}$ and $\varepsilon_{Eng}^{\{i\}}$ are the fitted engineering stress and the engineering strain at the end of an i-interval respectively.
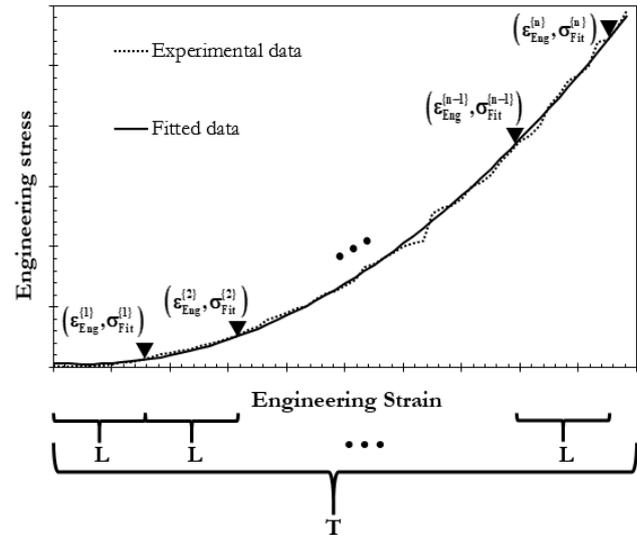
Fig. 5. Selection of the engineering stress-strain data.

Some hyperelastic constitutive models are generally written in a function of stretch ratio, the stretch ratio at the end of i-interval can be expressed as shown in Eq. (28).

$$\lambda^{\{i\}} = 1 + \varepsilon_{Eng}^{\{i\}} \qquad (28)$$

3.2.3. Determination material constants

The material constants of Neo-Hookean, Mooney-Rivlin, Yeoh, and Ogden can be solved with our proposed algorithm in form of a single equation or multiple equations.

A single equation:

The Neo-Hookean model has only one material constant C_{10} which can determine from the fitted engineering stress-strain data at $T/4$, $T/2$, $3T/4$, and T respectively. For the uniaxial testing data, the material constant C_{10} can be solved by substituting $\lambda = \lambda^{\{1\}}$ into Eq. (16) as shown in Eqs. (29)-(30).

$$\left[2\lambda^{\{1\}} - 2\left(\lambda^{\{1\}}\right)^{-2} \right] C_{10} = \sigma_{Fit}^{\{1\}} \qquad (29)$$

$$C_{10} = \frac{1}{2\lambda^{\{1\}} - 2\left(\lambda^{\{1\}}\right)^{-2}} \sigma_{Fit}^{\{1\}} \qquad (30)$$

Multiple equations:

Mooney-Rivlin and Yeoh models can separate material constants from the matrix formed by hyperelastic

constitutive models which is shown in Eq. (31) and solved by Eqs. (32)-(33).

$$\begin{bmatrix} \sigma_{model}\left(\lambda^{\{1\}}\right) \\ \sigma_{model}\left(\lambda^{\{2\}}\right) \\ \vdots \\ \sigma_{model}\left(\lambda^{\{n\}}\right) \end{bmatrix}_{n\,x\,1} \begin{bmatrix} C_{ij} \end{bmatrix}_{nxn} = \begin{bmatrix} \sigma_{Fit}^{\{1\}} \\ \sigma_{Fit}^{\{2\}} \\ \vdots \\ \sigma_{Fit}^{\{n\}} \end{bmatrix}_{n\,x\,1} \qquad (31)$$

where $\sigma_{model}\left(\lambda^{\{i\}}\right)$ is a function of the hyperelastic constitutive model at $\lambda^{\{i\}}$ (i start at 1 to n).

- **Mooney-Rivlin 3 parameter model**

$$\begin{bmatrix} M \end{bmatrix} \begin{bmatrix} C_{10} \\ C_{01} \\ C_{11} \end{bmatrix} = \begin{bmatrix} \sigma_{Fit}^{\{1\}} \\ \sigma_{Fit}^{\{2\}} \\ \sigma_{Fit}^{\{3\}} \end{bmatrix} \qquad (32)$$

$$\begin{bmatrix} C_{10} \\ C_{01} \\ C_{11} \end{bmatrix} = \begin{bmatrix} M \end{bmatrix}^{-1} \begin{bmatrix} \sigma_{Fit}^{\{1\}} \\ \sigma_{Fit}^{\{2\}} \\ \sigma_{Fit}^{\{3\}} \end{bmatrix} \qquad (33)$$

Elements of the matrix M are written as:

$$M_{11} = 2\lambda^{\{1\}} - 2\left(\lambda^{\{1\}}\right)^{-2} \qquad (34)$$

$$M_{12} = 2 - 2\left(\lambda^{\{1\}}\right)^{-3} \qquad (35)$$

$$M_{13} = 6\left(\lambda^{\{1\}}\right)^2 - 6\left(\lambda^{\{1\}}\right) + 6\left(\lambda^{\{1\}}\right)^{-2}$$
$$+ 6\left(\lambda^{\{1\}}\right)^{-3} - 6\left(\lambda^{\{1\}}\right)^{-4} - 6 \qquad (36)$$

$$M_{21} = 2\lambda^{\{2\}} - 2\left(\lambda^{\{2\}}\right)^{-2} \qquad (37)$$

$$M_{22} = 2 - 2\left(\lambda^{\{2\}}\right)^{-3} \qquad (38)$$

$$M_{23} = 6\left(\lambda^{\{2\}}\right)^2 - 6\left(\lambda^{\{2\}}\right) + 6\left(\lambda^{\{2\}}\right)^{-2}$$
$$+ 6\left(\lambda^{\{2\}}\right)^{-3} - 6\left(\lambda^{\{2\}}\right)^{-4} - 6 \qquad (39)$$

$$M_{31} = 2\lambda^{\{3\}} - 2\left(\lambda^{\{3\}}\right)^{-2} \qquad (40)$$

$$M_{32} = 2 - 2\left(\lambda^{\{3\}}\right)^{-3} \qquad (41)$$

$$M_{33} = 6\left(\lambda^{\{3\}}\right)^2 - 6\left(\lambda^{\{3\}}\right) + 6\left(\lambda^{\{3\}}\right)^{-2}$$
$$+ 6\left(\lambda^{\{3\}}\right)^{-3} - 6\left(\lambda^{\{3\}}\right)^{-4} - 6 \qquad (42)$$

Additionally, the Mooney-Rivlin n-parameter model has n material constants which required n selected data points. Thus, the matrix M has the size of n x n and each element of M is given in Eq. (17)-(19).

- **Yeoh 2nd order model**

$$\begin{bmatrix} Y \end{bmatrix} \begin{bmatrix} C_{10} \\ C_{20} \end{bmatrix} = \begin{bmatrix} \sigma_{Fit}^{\{1\}} \\ \sigma_{Fit}^{\{2\}} \end{bmatrix} \qquad (43)$$

Elements of the matrix Y are written as:

$$Y_{11} = 2\lambda^{\{1\}} - 2\left(\lambda^{\{1\}}\right)^{-2} \qquad (44)$$

$$Y_{12} = 4\left\{ \begin{bmatrix} \lambda^{\{1\}} - \left(\lambda^{\{1\}}\right)^{-2} \end{bmatrix} \\ \times \left[\left(\lambda^{\{1\}}\right)^2 + 2\left(\lambda^{\{1\}}\right)^{-1} - 3 \right] \right\} \qquad (45)$$

$$Y_{21} = 2\lambda^{\{2\}} - 2\left(\lambda^{\{2\}}\right)^{-2} \qquad (46)$$

$$Y_{22} = 4\left\{ \begin{bmatrix} \lambda^{\{2\}} - \left(\lambda^{\{2\}}\right)^{-2} \end{bmatrix} \\ \times \left[\left(\lambda^{\{2\}}\right)^2 + 2\left(\lambda^{\{2\}}\right)^{-1} - 3 \right] \right\} \qquad (47)$$

Additionally, the Yeoh 3rd order model has 3 material constants which required 3 selected data points. Thus, the matrix Y has the size of 3 x 3 and each element of Y is given in Eq. (20).

- **Ogden model**

In Ogden models, the material constants cannot be solved explicitly. For the PP algorithm, the Ogden models have 2, 4, and 6 material constants respectively which require to selected data points being equal to the number of material constants. Thus, each component of the stress vector is given in Eq. (48). For example, the Ogden 2nd order model has 4 material constants which required 4 selected data points, the material constants are acquired from Eq.(49) by using the Levenberg–Marquardt algorithm [17] which is well-known method to solve non-linear least squares problems.

$$\begin{bmatrix} \sum_{i=1}^{n} \mu_i \left(\left(\lambda^{\{1\}}\right)^{\alpha_i - 1} - \left(\lambda^{\{1\}}\right)^{-0.5\alpha_i - 1} \right) \\ \sum_{i=1}^{n} \mu_i \left(\left(\lambda^{\{2\}}\right)^{\alpha_i - 1} - \left(\lambda^{\{2\}}\right)^{-0.5\alpha_i - 1} \right) \\ \vdots \\ \sum_{i=1}^{n} \mu_i \left(\left(\lambda^{\{2n\}}\right)^{\alpha_i - 1} - \left(\lambda^{\{2n\}}\right)^{-0.5\alpha_i - 1} \right) \end{bmatrix} = \begin{bmatrix} \sigma_{Fit}^{\{1\}} \\ \sigma_{Fit}^{\{2\}} \\ \vdots \\ \sigma_{Fit}^{\{2n\}} \end{bmatrix} \qquad (48)$$

$$\begin{bmatrix} \left\{ \begin{array}{l} \mu_1\left(\left(\lambda^{\{1\}}\right)^{\alpha_1-1}-\left(\lambda^{\{1\}}\right)^{-0.5\alpha_1-1}\right) \\ +\mu_2\left(\left(\lambda^{\{1\}}\right)^{\alpha_2-1}-\left(\lambda^{\{1\}}\right)^{-0.5\alpha_2-1}\right) \end{array} \right\} \\ \left\{ \begin{array}{l} \mu_1\left(\left(\lambda^{\{2\}}\right)^{\alpha_1-1}-\left(\lambda^{\{2\}}\right)^{-0.5\alpha_1-1}\right) \\ +\mu_2\left(\left(\lambda^{\{2\}}\right)^{\alpha_2-1}-\left(\lambda^{\{2\}}\right)^{-0.5\alpha_2-1}\right) \end{array} \right\} \\ \left\{ \begin{array}{l} \mu_1\left(\left(\lambda^{\{3\}}\right)^{\alpha_1-1}-\left(\lambda^{\{3\}}\right)^{-0.5\alpha_1-1}\right) \\ +\mu_2\left(\left(\lambda^{\{3\}}\right)^{\alpha_2-1}-\left(\lambda^{\{3\}}\right)^{-0.5\alpha_2-1}\right) \end{array} \right\} \\ \left\{ \begin{array}{l} \mu_1\left(\left(\lambda^{\{4\}}\right)^{\alpha_1-1}-\left(\lambda^{\{4\}}\right)^{-0.5\alpha_1-1}\right) \\ +\mu_2\left(\left(\lambda^{\{4\}}\right)^{\alpha_2-1}-\left(\lambda^{\{4\}}\right)^{-0.5\alpha_2-1}\right) \end{array} \right\} \end{bmatrix} = \begin{bmatrix} \sigma_{Fit}^{\{1\}} \\ \sigma_{Fit}^{\{2\}} \\ \sigma_{Fit}^{\{3\}} \\ \sigma_{Fit}^{\{4\}} \end{bmatrix} \qquad (49)$$

Additionally, the Ogden 1st order model has 2 material constants which required 2 selected data points, and the Ogden 3rd order model has 6 material constants which required 6 selected data points; therefore, each element of the stress vector is defined in Eq. (48). Finally, material constants can then be obtained from the Levenberg–Marquardt algorithm.

3.3. Determination of Stability Regions

For incompressible materials, we assigned $\sigma_3 = d\sigma_3 = 0$ into Eq. (23); therefore the inequality is written as shown in Eq. (50).

$$d\sigma_1 d\varepsilon_1 + d\sigma_2 d\varepsilon_2 > 0 \qquad (50)$$

where σ_i is the Cauchy stress in the i-principal direction and ε_i is Cauchy strain in the i-principal direction. The changes of true strain are related to the stretch ratios which can be given in Eq. (51).

$$d\varepsilon_i = \frac{d\lambda_i}{\lambda_i} \qquad (51)$$

The relation between the changes of the Cauchy stress and the Cauchy strain can be formulated by the matrix equation as written in Eq. (52).

$$\begin{Bmatrix} d\sigma_1 \\ d\sigma_2 \end{Bmatrix} = \begin{bmatrix} D \end{bmatrix} \begin{Bmatrix} d\varepsilon_1 \\ d\varepsilon_2 \end{Bmatrix} \qquad (52)$$

where D is the tangential stiffness matrix and each element of D can be calculated from Eq. (53).

$$\begin{bmatrix} D \end{bmatrix} = \begin{bmatrix} \lambda_1 \dfrac{d\sigma_1}{d\lambda_1} & \lambda_2 \dfrac{d\sigma_1}{d\lambda_2} \\ \lambda_1 \dfrac{d\sigma_2}{d\lambda_1} & \lambda_2 \dfrac{d\sigma_2}{d\lambda_2} \end{bmatrix} \qquad (53)$$

Constitutive equations of the Neo-Hookean, Mooney-Rivlin and Yeoh models depend on the 1st and 2nd invariant; therefore, each elements of the symmetric matrix D can determine from Eq. (53).

Constitutive equation of the Ogden model depends only on the stretch ratio; therefore, each element of the symmetric matrix D is determined from Eqs. (54)–(56).

$$D_{11} = \sum_{i=1}^{N}\left(\mu_i\alpha_i\lambda_1^{\alpha_i} + \mu_i\alpha_i\lambda_1^{-\alpha_i}\lambda_2^{-\alpha_i}\right) \qquad (54)$$

$$D_{22} = \sum_{i=1}^{N}\left(\mu_i\alpha_i\lambda_2^{\alpha_i} + \mu_i\alpha_i\lambda_1^{-\alpha_i}\lambda_2^{-\alpha_i}\right) \qquad (55)$$

$$D_{12} = D_{21} = \sum_{i=1}^{N}\left(\mu_i\alpha_i\lambda_1^{-\alpha_i}\lambda_2^{-\alpha_i}\right) \qquad (56)$$

For material stability, the tangential stiffness matrix D must be positive definite which requires D to satisfied two conditions as written in Eqs. (57)-(58).

$$D_{11} + D_{22} > 0 \qquad (57)$$
$$D_{11}D_{22} - D_{12}D_{21} > 0 \qquad (58)$$

4. Results and Discussion

4.1. Determination of Material Constants

The material constants of hyperelastic models were determined from both the tensile and compressive testing data of the PDMS material. The *PP* algorithm was evaluated for its accuracy of reproducing stress-strain curves compared to ones of the ANSYS program and the uniaxial testing data.

4.1.1. Neo-Hookean model

The Neo-Hookean model has only one material constant C_{10}; therefore the fitted pairs of data have to carefully select as an input of the *PP* algorithm which are at $T/4$, $T/2$, $3T/4$, and T. Here, we found that *PP* algorithm obtained quite accurate results when L is $3T/4$. Finally, we found that *PP* algorithm obtains quite accurate prediction of stress-strain relationship under uniaxial testing. Comparison of tensile stress-strain curves reproduced from the *PP* algorithm for various L is shown in Fig. 6. Figure 7 shows comparison of compressive stress- strain reproduced from the *PP* algorithm for various L. Table 1 illustrates RSS between uniaxial testing data and data reproducing from the *PP* algorithm for various L. Figures 8 and 9 show comparison of tensile and compressive stress-strain curves, which generated from both the *PP* algorithm ($L = 3T/4$) and the ANSYS program. Tables 1-2 illustrate comparison of RSS between the uniaxial testing data and the data reproduced from the *PP* algorithm and the ANSYS program. Table 3 shows the material constant C_{10} determined from the uniaxial testing data by the *PP* algorithm and the ANSYS program.

Table 1. RSS between the uniaxial testing data and the data reproduced from the *PP* algorithm by the Neo-Hookean model.

Location of a selected data	RSS	
	Tensile test	Compressive test
$T/4$	483.20367	91.08280
$T/2$	307.98142	27.97998
$3T/4$	132.46641	9.17438
T	510.78097	20.15709

Table 2. RSS between the uniaxial testing data and the data reproduced from the ANSYS program and the *PP* algorithm (with fitted data at $3T/4$) by the Neo-Hookean model.

Type of data	RSS	
	ANSYS	*PP* algorithm
Tensile test	325.99015	132.46641
Compressive test	98.59628	9.17438

Table 3. The material constant C_{10} in the Neo-Hookean model determined from the uniaxial testing data by the *PP* algorithm (with fitted data at $3T/4$) and the ANSYS program.

Type of data	Neo-Hookean model	
	ANSYS	*PP* algorithm
Tensile test	0.45578	0.67085
Compressive test	0.12506	0.24041
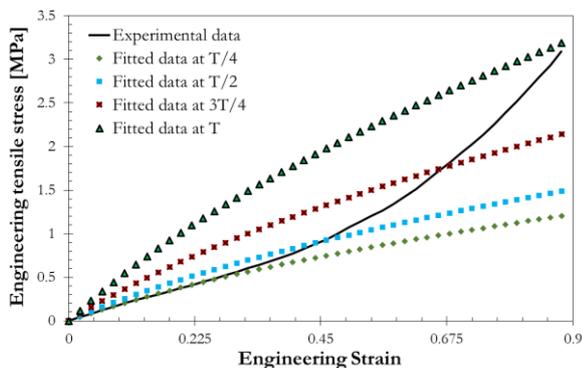
Fig. 6. Comparison of tensile stress-strain curves reproduced from the *PP* algorithm by the Neo-Hookean model to the tensile testing data.
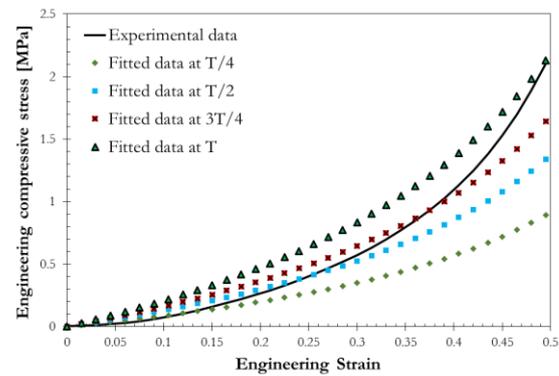
Fig. 7. Comparison of compressive stress-strain curves reproduced from the *PP* algorithm by the Neo-Hookean model to the compressive testing data.
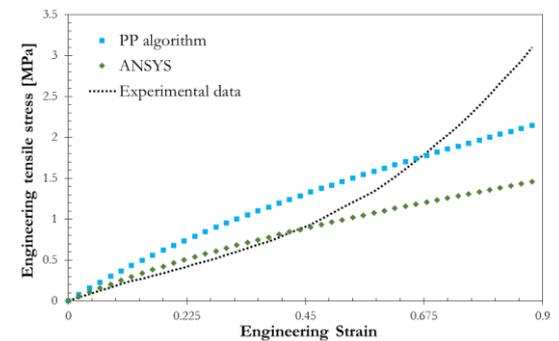
Fig. 8. Comparison of tensile stress-strain curves reproduced from the *PP* algorithm (with fitted data at $3T/4$) and the ANSYS program by the Neo-Hookean model to the tensile testing data.
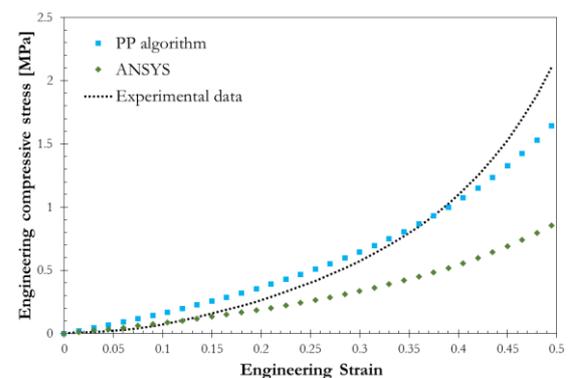
Fig. 9. Comparison compressive stress-strain curves reproduced from the *PP* algorithm (with fitted data at $3T/4$) and the ANSYS program by the Neo-Hookean model to the compressive testing data.

4.1.2. Mooney-Rivlin models

The Mooney-Rivlin 3, 5, and 9 parameters model had been studied to determine their material constants. Here, we found impressive reproducing results from the *PP* algorithm. Moreover, the Mooney-Rivlin 9 parameters model obtained the accurate model representing of the stress-strain curves with lowest RSS. Figures 10-12 show comparison of tensile stress-strain reproduced from the *PP* algorithm and the ANSYS program to the tensile testing data. Figures 13-15 show comparison of

compressive stress-strain reproduced from the *PP* algorithm and the ANSYS program to the compressive testing data. Tables 4-5 illustrates RSS between the uniaxial testing data and the data reproducing from the *PP* algorithm and the ANSYS program. As the number of parameters in the Mooney-Rivlin model increases, the accuracy of the constitutive model increases. Tables 6-7 show the material constants determined from the tensile testing data in the *PP* algorithm and the ANSYS program. Tables 8-9 shows the material constants determined from the compressive testing data in the *PP* algorithm and the ANSYS program respectively.

Table 4. RSS between the tensile testing data and the data reproduced from the *PP* algorithm and the ANSYS program by various Mooney-Rivlin models.

Mooney-Rivlin models	RSS	
	ANSYS	*PP* algorithm
3 parameters	2.30004	0.94446
5 parameters	0.12339	0.03349
9 parameters	0.05598	0.02348

Table 5. RSS between the compressive testing data and the data reproduced from the *PP* algorithm and the ANSYS program by various Mooney-Rivlin models.

Mooney-Rivlin models	RSS	
	ANSYS	*PP* algorithm
3 parameters	0.70566	0.14429
5 parameters	0.45302	0.00085
9 parameters	0.06440	0.00074

Table 6. The material constants in the Mooney-Rivlin models determined from the tensile testing data with the *PP* algorithm.

Material constants	Mooney-Rivlin models		
	Parameters		
	3	5	9
C_{10}	-1.83101	1.16746	-0.01920
C_{01}	2.52817	-0.86298	0.40418
C_{11}	0.76883	1.41975	-2241.08500
C_{20}		-0.04522	111.02655
C_{02}		-2.05832	113.60225
C_{30}			-0.38632
C_{21}			0.98571
C_{12}			-27.07851
C_{03}			11.46141

Table 7. The material constants in the Mooney-Rivlin models determined from the tensile testing data with the ANSYS program.

Material constants	Mooney-Rivlin models		
	Parameters		
	3	5	9
C_{10}	-0.54115	-0.46701	-9.79208
C_{01}	0.97146	0.88163	10.34925
C_{11}	0.49612	-3.91278	-246155.84137
C_{20}		1.54142	122917.86244
C_{02}		3.11667	123270.12261
C_{30}			505.37389
C_{21}			-3186.21598
C_{12}			-23261.11861
C_{03}			8036.22988

Table 8. The material constants in Mooney-Rivlin models determined from the compressive testing data with the *PP* algorithm.

Material constants	Mooney-Rivlin models		
	Parameters		
	3	5	9
C_{10}	-0.18295	-1.17299	-0.69856
C_{01}	0.28694	1.18820	0.73024
C_{11}	-0.01761	0.75693	-2097.97604
C_{20}		-1.13998	1052.14911
C_{02}		-0.18100	1046.16820
C_{30}			74.90284
C_{21}			-206.10185
C_{12}			-22.89094
C_{03}			3.527831

Table 9. The material constants in the Mooney-Rivlin models determined from the compressive testing data with the ANSYS program.

Material constants	Mooney-Rivlin models		
	Parameters		
	3	5	9
C_{10}	-0.44501	-0.16808	3.04478
C_{01}	0.50429	0.23398	-2.93246
C_{11}	-0.0622	-2.54487	-61745.70617
C_{20}		2.09914	30935.06855
C_{02}		0.78043	30821.49306
C_{30}			2095.10625
C_{21}			-5951.49632
C_{12}			-731.22547
C_{03}			113.39422
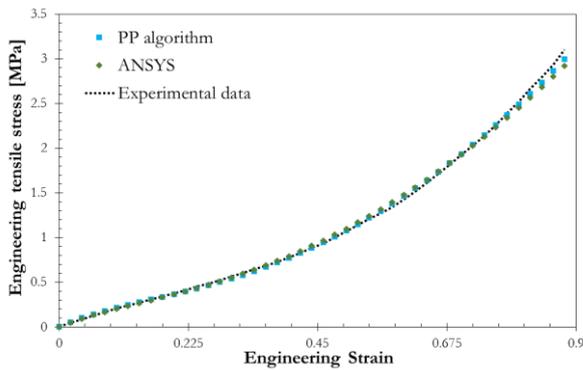
Fig. 10. Comparison of tensile stress-strain curves reproduced from the *PP* algorithm and the ANSYS program by the Mooney-Rivlin 3 parameters model to the tensile testing data.
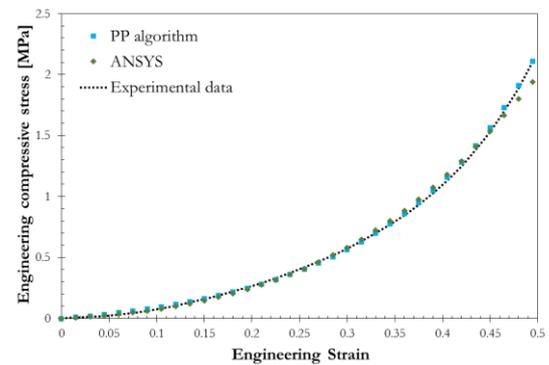
Fig. 11. Comparison of tensile stress-strain curves reproduced from the *PP* algorithm and the ANSYS program by the Mooney-Rivlin 5 parameters model to the tensile testing data.
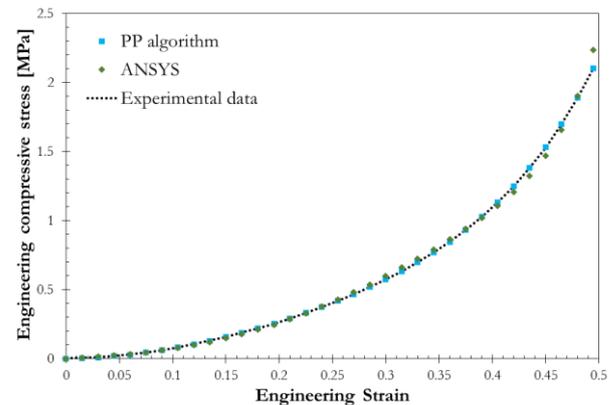
Fig. 12. Comparison of tensile stress-strain curves reproduced from the *PP* algorithm and the ANSYS program by the Mooney-Rivlin 9 parameters model to the tensile testing data.

Fig. 13. Comparison of compressive stress-strain curves reproduced from the *PP* algorithm and the ANSYS program by the Mooney-Rivlin 3 parameters model to the compressive testing data.

Fig. 14. Comparison of compressive stress-strain curves reproduced from the *PP* algorithm and the ANSYS program by the Mooney-Rivlin 5 parameters model to the compressive testing data.
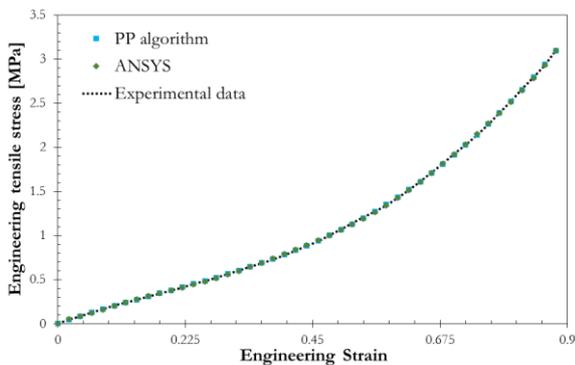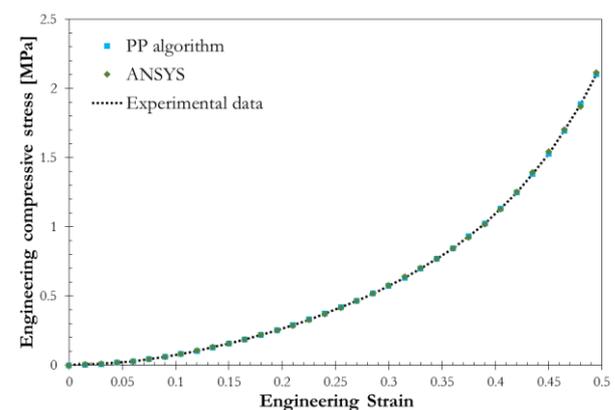
Fig. 15. Comparison of compressive stress-strain curves reproduced from the *PP* algorithm and the ANSYS program by the Mooney-Rivlin 9 parameters model to the compressive testing data.

4.1.3. Yeoh models

The *PP* algorithm obtained impressive results of reproduction of stress-strain curves. Figures 16-17 show comparison of tensile stress-strain curves reproduced from the *PP* algorithm and the ANSYS program to the tensile testing data. Figures 18-19 show comparison of

compressive stress-strain curves reproduced from the *PP* algorithm and the ANSYS program to the tensile testing data. Table 10 illustrates RSS between the tensile testing data and the data reproducing from the *PP* algorithm and the ANSYS program. Table 11 illustrates RSS between the compressive testing data and the data reproducing from the *PP* algorithm and the ANSYS program. As the order of the Yeoh model increases, the accuracy of the constitutive model increases. Tables 12-13 show the material constants determined from the tensile testing data and the compressive testing data by the *PP* algorithm and the ANSYS program respectively.
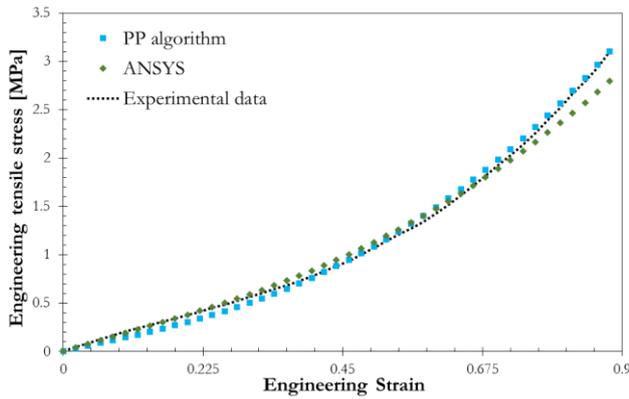
Fig. 16. Comparison of tensile stress-strain curves reproduced from the *PP* algorithm and the ANSYS program by the Yeoh 2nd order model to the tensile testing data.
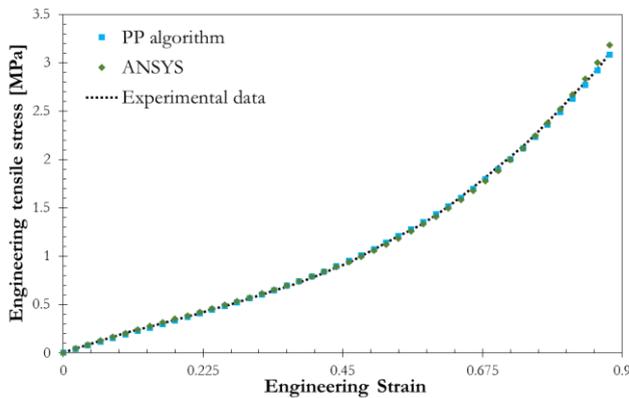
Fig. 17. Comparison of tensile stress-strain curves reproduced from the *PP* algorithm and the ANSYS program by the Yeoh 3rd order model to the tensile testing data.
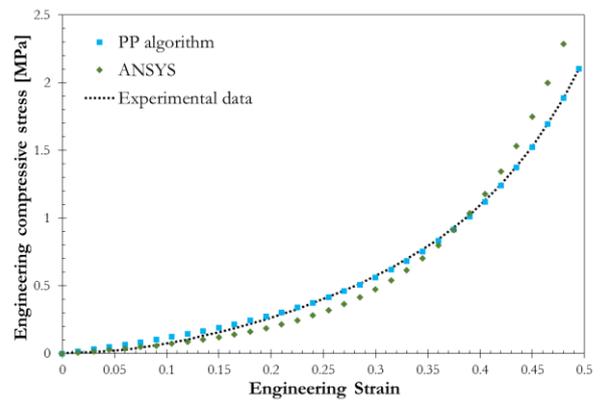
Fig. 18. Comparison of compressive stress-strain curves reproduced from the *PP* algorithm and the ANSYS program by the Yeoh 2nd order model to the compressive testing data.
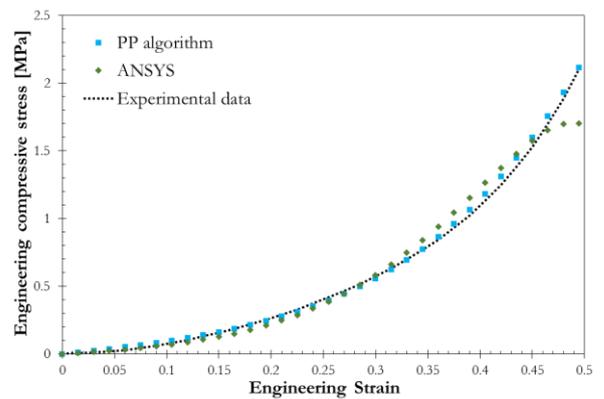
Fig. 19. Comparison of compressive stress-strain curves reproduced from the *PP* algorithm and the ANSYS program by the Yeoh 3rd order model to the compressive testing data.

Table 10. RSS between the tensile testing data and the data reproduced from the *PP* algorithm and the ANSYS program by various Yeoh Models.

Yeoh Models	RSS	
	ANSYS	*PP* algorithm
2nd order	7.90918	2.39860
3rd order	0.56914	0.18280

Table 11. RSS between the compressive testing data and the data reproduced from the *PP* algorithm and the ANSYS program by various Yeoh Models.

Yeoh Models	RSS	
	ANSYS	*PP* algorithm
2nd order	9.89472	0.22798
3rd order	4.18434	0.45872

Table 12. The material constants in the Yeoh models determined from the tensile testing data by the *PP* algorithm and the ANSYS program.

| Material constants | Yeoh models | | | |
| | 2nd order | | 3rd order | |
	ANSYS	*PP* algorithm	ANSYS	*PP* algorithm
C_{10}	0.33845	0.25126	0.36428	0.33892
C_{20}	0.16787	0.22521	0.07036	0.11533
C_{30}	-	-	0.05307	0.03365

Table 13. The material constants in the Yeoh models determined from the compressive testing data by the *PP* algorithm and the ANSYS program.

| Material constant | Yeoh models | | | |
| | 2nd order | | 3rd order | |
	ANSYS	*PP* algorithm	ANSYS	*PP* algorithm
C_{10}	0.09511	0.17019	0.08454	0.13591
C_{20}	0.11852	0.05661	0.24102	0.11755
C_{30}	-	-	-0.09507	-0.02520

4.1.4. Ogden models

With the *PP* algorithm, the Ogden 3rd order model was the accurate constitutive model for reproducing of stress-strain curves since it had the lowest RSS. Figures 20-22 show comparison of tensile stress-strain curves reproduced from the *PP* algorithm and the ANSYS program to the tensile testing data. Figures 23-25 show comparison of compressive stress-strain curves reproduced from the *PP* algorithm and the ANSYS program to the compressive testing data. Table 14 illustrates RSS between the tensile testing data and the data reproducing from the *PP* algorithm and the ANSYS program. Table 15 illustrates RSS between the compressive testing data and the data reproducing from the *PP* algorithm and the ANSYS program. As the order of the Ogden model increases, the accuracy of the constitutive model increases. Tables 16-17 show the material constants determined from the tensile testing data by the *PP* algorithm and the ANSYS program respectively. Tables 18-19 show the material constants determined from the compressive testing data by the *PP* algorithm and the ANSYS program respectively.

Table 14. RSS between the tensile testing data and the data reproduced from the *PP* algorithm and the ANSYS program with the Ogden models.

| Ogden Models | RSS | |
	ANSYS	*PP* algorithm
1st order	9.13155	1.17705
2nd order	0.56855	0.15337
3rd order	0.03369	0.02966

Table 15. RSS between the compressive testing data and the data reproduced from the *PP* algorithm and the ANSYS program by various Ogden models.

| Ogden Models | RSS | |
	ANSYS	*PP* algorithm
1st order	72.61336	0.12535
2nd order	78.38356	0.11588
3rd order	78.13855	0.11570

Table 16. The material constants in the Ogden model determined from the tensile testing data by the *PP* algorithm.

| Material constants | Ogden models | | |
	1st order	2nd order	3rd order
μ_1	0.17666	56.05795	47.19930
α_1	5.54368	0.01435	2.08600
μ_2		0.07938	-78.36774
α_2		6.57819	2.57958
μ_3			35.21105
α_3			2.98970

Table 17. The material constants in the Ogden models determined from the tensile testing data with the ANSYS program.

| Material constants | Ogden models | | |
	1st order	2nd order	3rd order
μ_1	0.26299	0.04102	-149.35934
α_1	4.75275	7.57032	0.30898
μ_2		422.57243	0.26001
α_2		0.00276	5.29229
μ_3			494.13556
α_3			0.09382

Table 18. The material constants in the Ogden models determined from the compressive testing data by the *PP* algorithm.

| Material constants | Ogden models | | |
	1st order	2nd order	3rd order
μ_1	-0.25722	-0.12413	-0.07254
α_1	-2.23321	-2.27832	-2.28350
μ_2		-0.12412	-0.07255
α_2		-2.27831	-2.28349
μ_3			-0.10215
α_3			-2.28322

Table 19. The material constants in the Ogden models determined from the compressive testing data by the ANSYS program.

Material constants	Ogden models		
	1st order	2nd order	3rd order
μ_1	12397.06910	5.11284	4.36077
α_1	0.00004	0.04722	0.03681
μ_2		5.11285	4.36085
α_2		0.04713	0.03693
μ_3			4.36099
α_3			0.03688
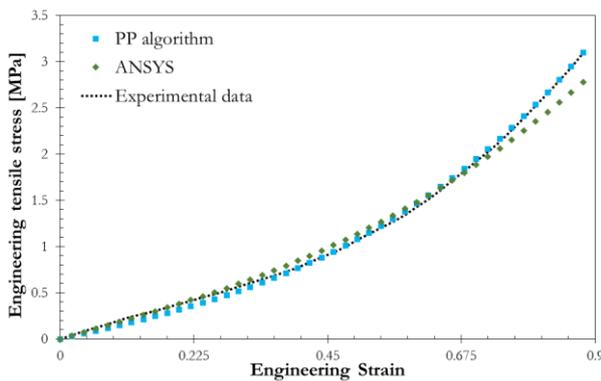
Fig. 20. Comparison of tensile stress-strain curves reproduced from the *PP* algorithm and the ANSYS program by the Ogden 1st order model to the tensile testing data.
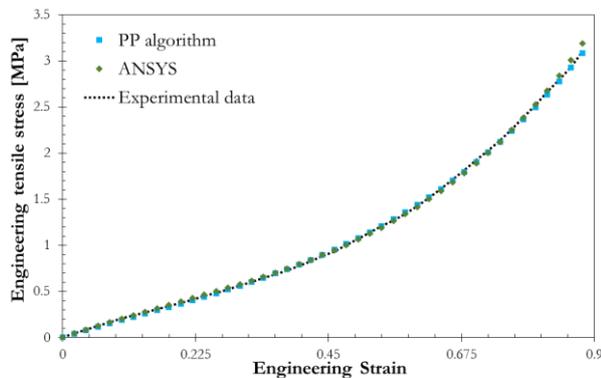
Fig. 21. Comparison of tensile stress-strain curves reproduced from the *PP* algorithm and ANSYS program by the Ogden 2nd order model with the tensile testing data.
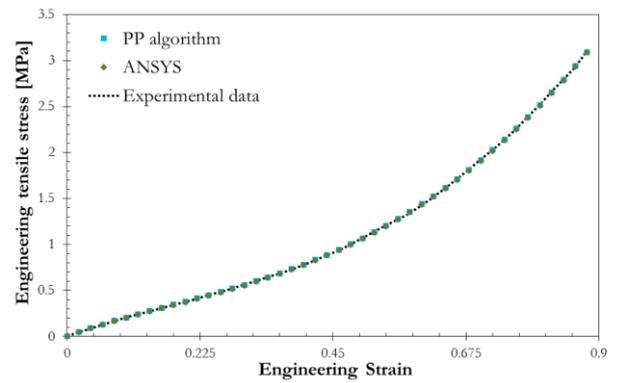
Fig. 22. Comparison of tensile stress-strain curves reproduced from the *PP* algorithm and the ANSYS program by the Ogden 3rd order model to the tensile testing data.
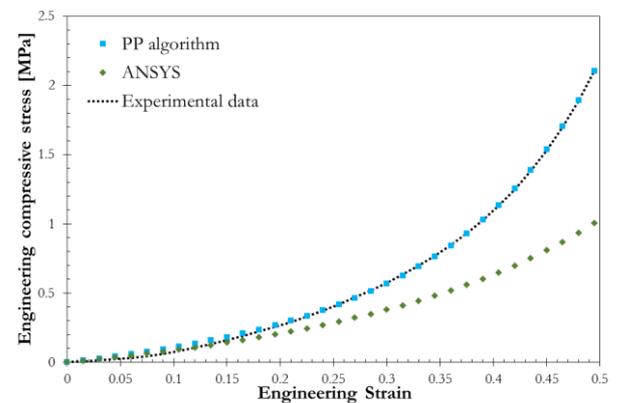
Fig. 23. Comparison of compressive stress-strain curves reproduced from the *PP* algorithm and the ANSYS program by the Ogden 1st order model to the compressive testing data.
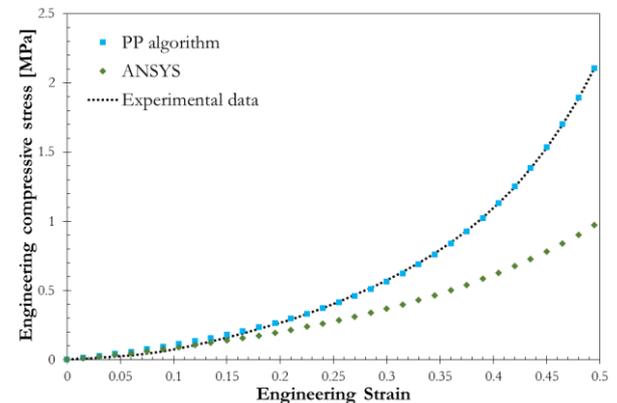
Fig. 24. Comparison of compressive stress-strain curves reproduced from the *PP* algorithm and the ANSYS program by the Ogden 2nd order model to the compressive testing data.
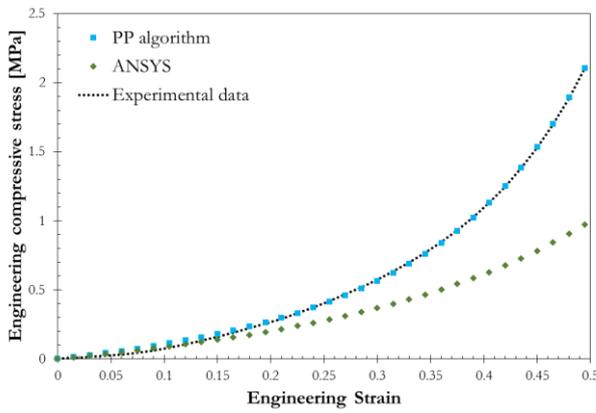
Fig. 25. Comparison of compressive stress-strain curves reproduced from the *PP* algorithm and the ANSYS program by the Ogden 3rd order model to the compressive testing data.

4.2. Stability Regions

The Drucker stability of constitutive models for the first three modes of deformation of various hyperelastic models and loading conditions are listed in Tables 20-23. Here, the *PP* algorithm and the ANSYS program obtained the comparable strain range limit. Nonetheless, the computational error on the strain range limit from ANSYS was found in the Yeoh 3rd order model obtained from the compressive testing data. The plots of the trace and the determinant of the tangential stiffness matrix *D* for various compressive engineering strains are shown in Figs. 26-27. It was found that the exact unstable condition occurred when ε_{Eng} < -0.472. In the Drucker stability criterion, the strain limit range depends on both the trace and the determinant of the tangential stiffness matrix [*D*] to be positive definite. They imply that the partial derivative of stress with respect to stretch ratio in the 1st and 2nd principal directions must be both positive while the *PP* algorithm determines the material constants from the 1st principal direction. Figures 28-29 show that the 5 and 9 parameter Mooney-Rivlin models had the negative D_{22} (the slope in the 2nd principal direction) by both the *PP* algorithm and the ANSYS program.

Table 20. Unstable conditions of various hyperelastic models obtained from the tensile testing data by the *PP* algorithm.

Models	Unstable conditions		
	Uniaxial	Equibiaxial	Planar
Neo-Hooken	None	None	None
Mooney-Rivlin:			
3 parameters	None	ε_{Eng} > 0.112	None
5 parameters	ε_{Eng} > 0.125	ε_{Eng} > 0.046	ε_{Eng} > 0.089
9 parameters	ε_{Eng} > 0.154	ε_{Eng} > 0.067	ε_{Eng} > 0.116
Yeoh:			
2nd order	None	None	None
3rd order	None	None	None
Ogden:			
1st order	None	None	None
2nd order	None	None	None
3rd order	None	None	None

Table 21. Unstable conditions of various hyperelastic models obtained from the tensile testing data by the ANSYS program.

Models	Unstable conditions		
	Uniaxial	Equibiaxial	Planar
Neo-Hooken	None	None	None
Mooney-Rivlin:			
3parameters	None	None	None
5parameters	ε_{Eng} > 1.330	ε_{Eng} > 0.200	None
9parameters	ε_{Eng} > 0.040	ε_{Eng} > 0.010	ε_{Eng} > 0.040
Yeoh:			
2nd order	None	None	None
3rd order	None	None	None
Ogden:			
1st order	None	None	None
2nd order	None	None	None
3rd order	None	None	None

Table 22. Unstable conditions of various hyperelastic models given from the compressive testing data by the *PP* algorithm.

Models	Unstable conditions		
	Uniaxial	Equibiaxial	Planar
Neo-Hookean	None	None	None
Mooney-Rivlin:			
3 parameters	$\varepsilon_{Eng} <$ -0.193	$\varepsilon_{Eng} <$ -0.096	None
5 parameters	$\varepsilon_{Eng} <$ -0.007	$\varepsilon_{Eng} <$ -0.004	$\varepsilon_{Eng} <$ -0.006
9 parameters	$\varepsilon_{Eng} <$ -0.021	$\varepsilon_{Eng} <$ -0.014	$\varepsilon_{Eng} <$ -0.020
Yeoh:			
2nd order	None	None	None
3rd order	None	$\varepsilon_{Eng} <$ -0.302	$\varepsilon_{Eng} <$ -0.492
Ogden:			
1st order	None	None	None
2nd order	None	None	None
3rd order	None	None	None

Table 23. Unstable conditions of hyperelastic models obtained from the compressive testing data by the ANSYS program.

Models	Unstable conditions		
	Uniaxial	Equibiaxial	Planar
Neo-Hookean	None	None	None
Mooney-Rivlin:			
3 parameters	$\varepsilon_{Eng} <$ -0.060	$\varepsilon_{Eng} <$ -0.029	$\varepsilon_{Eng} <$ -0.051
5 parameters	$\varepsilon_{Eng} <$ -0.506	$\varepsilon_{Eng} <$ -0.175	$\varepsilon_{Eng} <$ -0.318
9 parameters	$\varepsilon_{Eng} <$ -0.032	$\varepsilon_{Eng} <$ -0.009	$\varepsilon_{Eng} <$ -0.032
Yeoh:			
2nd order	None	None	None
3rd order	None	None	None
Ogden:			
1st order	None	None	None
2nd order	None	None	None
3rd order	None	None	None

Fig. 26. Comparison $D_{11} + D_{22}$ of the Yeoh 3rd order model obtained from the *PP* algorithm and the ANSYS program.
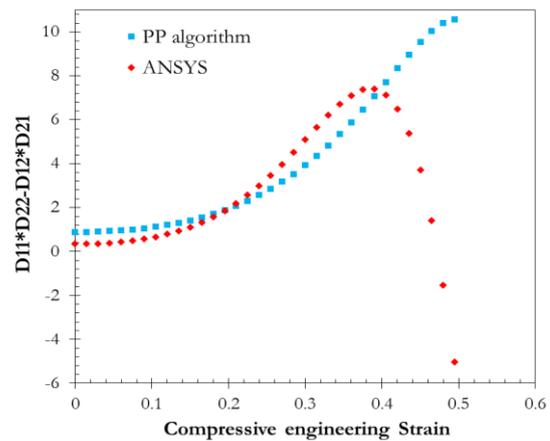
Fig. 27. Comparison $D_{11}D_{22} - D_{12}D_{21}$ of the Yeoh 3rd order model obtained from the *PP* algorithm and the ANSYS program.
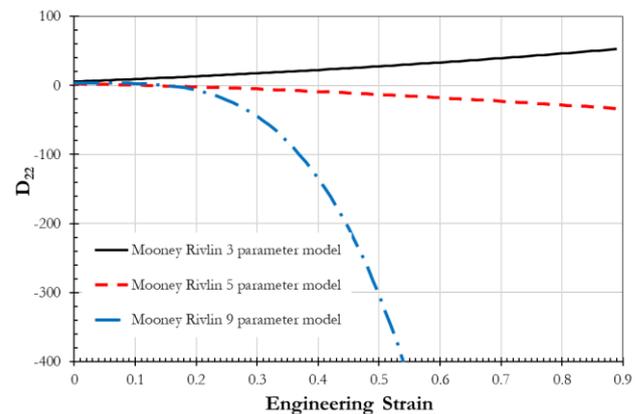
Fig. 28. Plot of D_{22} and engineering strain for various Mooney-Rivlin models by the *PP* algorithm.
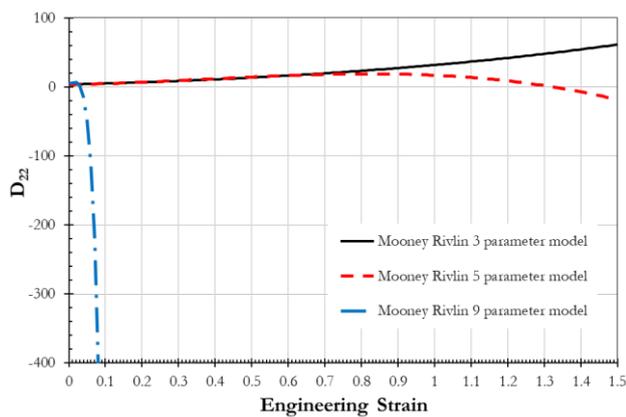
Fig. 29. Plot of D_{22} and engineering strain for various Mooney-Rivlin models by the *PP* algorithm.

5. Conclusions

In this research, the *PP* algorithm was proposed for determining material constants and strain limit ranges from 3, 5, and 9 parameter Neo-Hookean; Mooney-Rivlin; 2nd and 3rd order Yeoh; and 1st, 2nd, and 3rd order Ogden. Moreover, the accuracies of engineering stress-strain curve reproduction were determined from RSS between the uniaxial testing data and the hyperelastic models and were evaluated with ones of the commercial finite element program, ANSYS. In the Neo-Hookean and Ogden models, the *PP* algorithm effectively determined material constants from the uniaxial testing data of the PDMS material in which their RSSs were lower than ones from the ANSYS program while the strain limit ranges were comparable. However, in Mooney-Rivlin and Yeoh models, the *PP* algorithm obtained lower RSS between the uniaxial testing data and the hyperelastic models but had smaller strain limit ranges than ones from ANSYS. Since their strain limit ranges were highly sensitive to their material constants. Therefore, it will need to improve the *PP* algorithm to have abilities to simultaneously optimize both RSS between the testing data and the hyperelastic models and the strain limit range (D_{11} and D_{22}) which would achieve both wider strain limit ranges and the accurate and acceptable RSS. Additionally, by nature of hyperelastic constitutive models, the higher is the order of the hyperelastic constitutive model, the lower is the RSS and the narrower is the strain limit range. Finally, the most accurate constitutive model for PDMS is the Ogden 3rd order model since it obtained not only low RSS but also no strain range limit.

Acknowledgement

References

[1] A. Ali, M. Hosseini, and B. B. Sahari, "A review of constitutive models for rubber-like materials," *American J. Engineering and Applied Sciences*, vol. 3, no. 1, pp. 232-239, Jan. 2010.

[2] J. A. López-Campos, A. Segade, E. Casarejos, J. R. Fernández, and G. R. Días, "Hyperelastic characterization oriented to finite element applications using genetic algorithms," *Advances in Engineering Software*, vol. 133, pp. 52-59, Apr. 2019.

[3] S. Kindo, R. Vashistha, S. Raj, G. P. Ravishankar, and M. P. Padwale, "Selection and validation of hyperelastic finite element model for analysis of silicone rubber," in *AIP Conference Proceedings 1978*, Thessaloniki, Greece, 2017, p. 470006.

[4] R. Tobajas, D. Elduque, C. Javierre, E. Ibarz, and L. Gracia, "A comparative study of hyperelastic constitutive models for an automotive shaft seal material," *Inter. J. Service and Computing Oriented Manufacturing*, vol. 3, no. 2. pp. 171-189, 2018.

[5] M. R. Mansouri and H. Darijani, "Constitutive modeling of isotropic hyperelastic materials in an exponential framework using a self-contained approach," *Inter. J. Solids and Structures*, vol. 51, no. 25 pp. 4316-4326, Sept. 2014.

[6] Y. Gorash, T. Comlekci, and R. Hamilton, "CAE-based application for identification and verification of hyperelastic parameters," *Proc. IMechE. Part L: J. Materials: Design and Applications*, vol. 231, no. 7, pp. 611-626, Sep. 2015.

[7] N. Kumar and V. V. Rao, "Hyperelastic Mooney-Rivlin model: Determination and physical interpretation of material constants," *MIT Inter. J. Mechanical Engineering*, vol. 6, no. 1, pp. 43-46, Jan. 2016.

[8] G. Marckmann and E. Verron, "Comparison of hyperelastic models for rubber-like materials," *Rubber Chemistry and Technology*, vol. 79, no. 5, pp. 835-858, Nov. 2006.

[9] E. Elgström, "Practical implementation of hyperelastic material methods in FEA models," *M. Engineering*, BTH, Karlskrona, Sweden, 2014.

[10] S. Iniguez-Macedo, R. Lostado-Lorza, R. Escribano-Garcia, and M. A. Martinez-Calvo, "Finite element model updating combined with multi-response optimization for hyper-elastic materials characterization," *Materials*, vol. 12, no. 7, pp. 1019, Mar. 2019.

[11] B. Kim, S. B. Lee, J. Lee, S. Cho, H. Park, S. Yeom, and S. H. Park, "A comparison among Neo-Hookean model, Mooney-Rivlin model, and Ogden model for chloroprene rubber," *Inter. J. Precision Engineering and Manufacturing*, vol. 13, no. 5, pp. 759-764, May 2012.

[12] L. Ruggiero, H. Sol, H. Sahli, S. Adriaenssens, and N. Adriaenssens, "An Inverse Method to Determine Material Properties of Soft Tissues," in *Mechanics of Biological Systems and Materials*. New York: Springer, 2011, ch. 3, pp. 19-32.

[13] M. R. Mansouri, H. Darijani, and M. Baghani, "On the correlation of FEM and experiments for

hyperelastic elastomers," *Experimental Mechanics*, vol. 57, no. 2, pp. 195-206, Oct. 2016.

[14] C. Liu, C. M. Cady, M. L. Lovato, and E. B. Orler, "Uniaxial tension of thin rubber liner sheets and hyperelastic model investigation," *J. Materials Science*, vol. 50, no. 3, pp. 1401-1411, Nov. 2015.

[15] M. Pawlikowski, "Non-linear approach in visco-hyperelastic constitutive modelling of polyurethane nanocomposite," *Mechanics of Time-Dependent Materials*, vol. 18, no. 1, pp. 1-20, Feb. 2013.

[16] H. Zhong and T. Peters, "A real time hyperelastic tissue model," *Computer Methods in Biomechanics and Biomedical Engineering*, vol. 10, no. 3, pp. 185-193, Jun. 2007.

[17] Y. Wang, Z. Ma, and L. Wang, "A finite element stratification method for a polyurethane jounce bumper," *Proc. IMechE. Part D: J. Automobile Engineering*, vol. 230, no. 7, pp. 983-992, Jul. 2015.

[18] J. Oden and Y. Fung, "Determination of material parameters from test data," in *Nonlinear Finite Element Analysis of Elastomers*. California: White Paper: MSC Software, 2010, ch. 3, pp. 20-21.

[19] K. Upadhyay, G. Subhash, and D. Spearot, "Thermodynamics-based stability criteria for constitutive equations of isotropic hyperelastic solids," *J. the Mechanics and Physics of Solids*, vol. 124, pp. 115-142, Oct. 2018.

[20] I. Liu, "A note on the Mooney–Rivlin material model," *Continuum Mechanics and Thermodynamics*, vol. 24, no. 4, pp. 583-593, Feb. 2012.

[21] K. Thanakhun and T. Puttapitukporn, "PDMS material models for anti-fouling surfaces using finite element method," *Engineering Journal*, vol. 23, no. 6, pp. 381-398, Nov. 2019.

[22] T. Pakawan and T. Puttapitukporn, "Compressive behaviors of micropillar sheets made of PDMS material using the finite element method," *Engineering Journal*, vol. 24, no. 4, Jul. 2020.

Jate Phothiphatcha received the B.Eng. degree in mechanical engineering from Kasetsart University, Thailand in 2017.

Tumrong Puttapitukporn received the B.Eng. degree in mechanical engineering from Kasetsart University, Thailang in 1998, and the M.S. and Ph.D. degree in mechanical engineering from Oregon State University, USA in 1999 and 2003 repectively.

He is currently the Associate Professor in Department of Mechanical Engineering, Kasetsat university, Thailand. His researach focus on finite element modeling and applications of generalized continuum theories.